# Switching between Inner- and Outer-Sphere PCET Mechanisms of Small-Molecule Activation: Superoxide Dismutation and Oxygen/Superoxide Reduction Reactivity Deriving from the Same Manganese Complex

Isabell Kenkel,[†] Alicja Franke,[†] Maximilian Dürr,[†] Achim Zahl,[†] Carlos Dücker-Benfer,[†] Jens Langer,[†] Milos R. Filipović,[†] Meng Yu,[‡] Ralph Puchta,[†] Stephanie R. Fiedler,[§] Matthew P. Shores,[§] Christian R. Goldsmith,*[,‡] and Ivana Ivanović-Burmazović*[,†]

[†]Department of Chemistry and Pharmacy, University Erlangen-Nuremberg, 91058 Erlangen, Germany
[‡]Department of Chemistry and Biochemistry, Auburn University, Auburn, Alabama 36849, United States
[§]Department of Chemistry, Colorado State University, Fort Collins, Colorado 80523-1872, United States

Ⓢ *Supporting Information*

**ABSTRACT:** Readily exchangeable water molecules are commonly found in the active sites of oxidoreductases, yet the overwhelming majority of studies on small-molecule mimics of these enzymes entirely ignores the contribution of water to the reactivity. Studies of how these enzymes can continue to function in spite of the presence of highly oxidizing species are likewise limited. The mononuclear $Mn^{II}$ complex with the potentially hexadentate ligand $N$-(2-hydroxy-5-methylbenzyl)-$N,N',N'$-tris(2-pyridinylmethyl)-1,2-ethanediamine ($L^{OH}$) was previously found to act as both a $H_2O_2$-responsive MRI contrast agent and a mimic of superoxide dismutase (SOD). Here, we studied this complex in aqueous solutions at different pH values in order to determine its (i) acid–base equilibria, (ii) coordination equilibria, (iii) substitution lability and operative mechanisms for water exchange, (iv) redox behavior and ability to participate in proton-coupled electron transfer (PCET) reactions, (v) SOD activity and reductive activity toward both oxygen and superoxide, and (vi) mechanism for its transformation into the binuclear $Mn^{II}$ complex with $^{(H)O}L–L^{OH}$ and its hydroxylated derivatives. The conclusions drawn from potentiometric titrations, low-temperature mass spectrometry, temperature- and pressure-dependent $^{17}O$ NMR spectroscopy, electrochemistry, stopped-flow kinetic analyses, and EPR measurements were supported by the structural characterization and quantum chemical analysis of proposed intermediate species. These comprehensive studies enabled us to determine how transiently bound water molecules impact the rate and mechanism of SOD catalysis. Metal-bound water molecules facilitate the PCET necessary for outer-sphere SOD activity. The absence of the water ligand, conversely, enables the inner-sphere reduction of both superoxide and dioxygen. The $L^{OH}$ complex maintains its SOD activity in the presence of •OH and $Mn^{IV}$-oxo species by channeling these oxidants toward the synthesis of a functionally equivalent binuclear $Mn^{II}$ species.
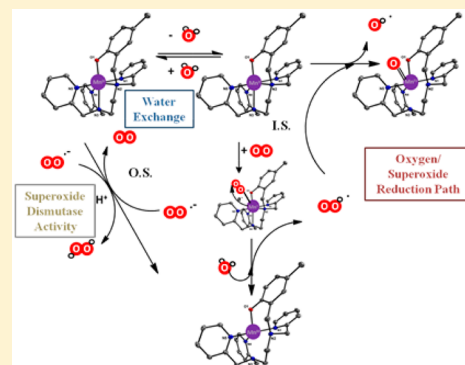
## INTRODUCTION

Determining the factors that control the solution behavior and redox reactivity of metal centers is essential both for optimizing small-molecule catalysts and for understanding the operation of metal-containing oxidoreductases. Small-molecule models have long been used in bioinorganic chemistry to provide insight into how metalloenzymes function. In these models, a polydentate ligand is commonly used to approximate the peptide-derived coordination sphere provided by the enzyme. Most synthetic efforts have focused on making changes to the polydentate ligand in order to modulate the geometry, stereochemistry, and overall charge of the metal complexes; the identities of the donor atoms; and the rigidity/flexibility and

bulkiness of the ligands, and each of these has been demonstrated to impact the reactivity of the metal centers.[1]

There is evidence that the primary ligand sphere, however, is not the sole determinant of activity, that crucial contributions may come from interactions with solvent molecules, and that these interactions can be tuned via acid–base equilibria.[2] Many oxidoreductases are believed to function via proton-coupled electron transfer (PCET) mechanisms that rely on water/hydroxide/oxide ligands to provide or abstract the protons and to modulate the redox potentials of the involved metal ions. An excellent illustration of the impact of the coordinated solvent

molecules ($H_2O$ or $OH^-$) on the redox properties of biologically relevant metal centers is provided by Mn and Fe superoxide dismutase (SOD) enzymes and their Fe- or Mn-substituted analogues.[3−6] Even though these interactions are widely acknowledged to be important, most small-molecule mimics do not contain coordinated water molecules and are studied in nonaqueous solutions. The active sites of SOD enzymes, for instance, are often approximated by hexa- and heptacoordinate Mn complexes with polydentate amino-pyridines and one or more monodentate ligands;[2,7,8] these monodentate ligands, usually MeCN or $Cl^-$ (neither of which is found in the native enzyme), remain coordinated in non-aqueous solutions.[2] Although such studies nicely illustrate how changes to the pyridylamine ligand influence the redox properties of the bound Mn related to SOD activity, they do not address how the coordination of water can mediate its reactivity.[2]

That motivated us to study the aqueous chemistry of the $[(L^{OH})Mn^{II}(solv)](ClO_4)_2$ complex (1), where $L^{OH}$ is the potentially hexadentate ligand $N$-(2-hydroxy-5-methylbenzyl)-$N,N',N'$-tris(2-pyridinylmethyl)-1,2-ethanediamine. The ligand is closely related to the pyridylamine ligands used in the aforementioned studies[2] and can be thought of as a close analogue of $N,N,N',N'$-tetrakis(2-pyridylmethyl)-1,2-ethanedi-amine (tpen).[9] The $L^{OH}$ and tpen ligands differ in that the former contains a phenol in place of one of the pyridine moieties; the phenol may approximate the tyrosine found in the active sites of Mn and Fe SODs.[10] Despite the lack of a macrocyclic component or a carboxylate group, the $Mn^{II}$ complex with $L^{OH}$ was found to be stable enough in water to serve as a $H_2O_2$-responsive contrast agent for magnetic resonance imaging (MRI).[11] The hexadenticity, coupled with the ability of $Mn^{II}$ to accommodate heptacoordination, allows for the binding of a single monodentate ligand. Subsequent work suggested that 1 may serve as a functional mimic of SOD.[12]

In order to better understand the solution behavior and reactivity of bioinorganic model systems in aqueous solutions, we have conducted a more thorough study of 1. We have assessed the water exchange dynamics of the $Mn^{II}$-bound water molecule, the speciation of 1 between various six- and seven-coordinate complexes, the redox activity as a function of pH, and the reactivity with superoxide and dioxygen. One of our groups previously reported that the $L^{OH}$ ligand in 1 undergoes oxidative coupling upon reaction with $H_2O_2$ in either MeCN or water to yield the binuclear complex $[(^{HO}L-L^{O-})-Mn^{II}_2(solv)_2](ClO_4)_3$ (2).[11] Here, we demonstrate that this coupling reaction protects the catalytic sites from the reactive oxygen species (ROS) and $Mn^{IV}$-oxo species that are produced outside of the mechanism that is predominantly responsible for SOD mimicry. Instead of degrading and deactivating the mononuclear complex, these oxidants transform it into the more stable 2, which displays SOD activity that is comparable to two equiv of 1.

The ability of 1 to toggle between catalytic superoxide dismutation and the reduction of oxygen to yield ROS and $Mn^{IV}$-oxo species is, to the best of our knowledge, unique. The reactivity switches between outer- (OS) and inner-sphere (IS) PCET mechanisms of small-molecule activation. Whether the OS or IS mechanism is operable is determined by the coordination equilibrium between seven- and six-coordinate $[(L^{O-})Mn^{II}(OH_2)]^+$ and $[(L^{O-})Mn^{II}]^+$ species and the lesser lability of the related five-coordinate $[(L^{O-})Mn^{III}(OH^-)]^+$ form

present in the catalytic cycle responsible for superoxide dismutation. The role of the coordination equilibrium is reminiscent of the reactivity of the Mn SOD enzyme in that its catalytic cycle is proposed to alternate between six- and five-coordinate active sites.[13−15] The observed mechanistic behavior was compared to that of one of the most efficient classes of MnSOD mimetics, i.e., pentaazamacrocyclic SOD mimetics,[7,16] that also exhibit coordination equilibria between hepta- and hexacoordinate species, and general conclusions were drawn.

## ■ EXPERIMENTAL SECTION

**Materials and Instrumentation.** Except where noted otherwise, chemicals were purchased from Sigma-Aldrich and used as received. Anhydrous acetonitrile (MeCN) was purchased from Acros Organics and stored in a glovebox free of moisture and oxygen. Hydrogen peroxide ($H_2O_2$, 50 wt %) was bought from Fisher. Dry nitrogen ($N_2$) and oxygen ($O_2$) were purchased from Airgas. $N$-(2-Hydroxy-5-methylbenzyl)-$N,N',N'$-tris(2-pyridinylmethyl)-1,2-ethanediamine ($L^{OH}$), $[(L^{OH})Mn^{II}(MeCN)](ClO_4)_2$ (1), and $[(^{HO}L−L^{O-})-Mn^{II}_2(MeCN)_2](ClO_4)_3$ (2) were prepared as previously described.[11] Deionized Millipore water was used for all aqueous measurements. All buffers were treated with Chelex sodium exchange resin to remove all trace metals.

**Determination of in Vitro SOD Activity via Stopped-Flow Technique.** Superoxide dismutase activity was tested by a direct method using a stopped-flow technique described elsewhere.[17] Experiments were carried out on a Biologic SFM-400 instrument, using syringes 1, 2, and 3, equipped with an Energetiq LDLS ENQ EQ-99-FC laser-driven light source and a J&M TIDAS diode array detector (integration time 0.5 ms, $\lambda$ = 180−724 nm). The source of superoxide was commercially available $KO_2$ dissolved in dry DMSO ($[O_2^{\bullet-}] \approx 1−2$ mM). Each complex was tested at four different concentrations between 0.9 and 9 $\mu$M in aqueous solutions buffered with HEPES or sodium phosphate to either pH 7.4 or pH 8.1. The aqueous solution containing the $Mn^{II}$ complex was mixed in a 9:1 ratio with the superoxide solution in DMSO using a high-density mixer. In each experiment, the concentration of superoxide exceeded that of the $Mn^{II}$ complex by at least 10-fold in order to ensure catalytic conditions. Millipore water was used for the preparation of the buffer solutions; the buffers were treated with Chelex 100 sodium exchange resin for at least 12 h before use in order to remove adventitious metal ions. The data analysis was performed using BioKine V4.66 software. Each reported $k_{obs}$ value is the average of at least 10 measurements. $k_{cat}$ values were determined from the slope of the $k_{obs}$ vs [Mn] plot.

**Cryo-MS Measurements.** Cryospray-ionization MS (CSI-MS) measurements were performed on a UHR-TOF Bruker Daltonik (Bremen, Germany) maXis plus, an ESI-quadrupole-time-of-flight (qToF) mass spectrometer capable of resolution of at least 60 000 fwhm, which was coupled to a Bruker Daltonik Cryospray unit. Detection was in positive-ion mode, with a source voltage of 4.5 kV. The flow rates were 250 $\mu$L/h. Both the $N_2$ drying gas ($N_2$), which aided solvent removal, and the spray gas were maintained at temperatures of 5 °C for aqueous solutions. For MeCN solutions, the temperature of drying gas was kept at −20 °C and the spray gas at −40 °C. The machine was calibrated prior to each experiment via direct infusion of the Agilent ESI-TOF low concentration tuning mixture, which provided an $m/z$ range of singly charged peaks up to 2700 Da in both ion modes.

**Cyclic Voltammetry.** Redox potentials were determined on an Autolab instrument equipped with a PGSTAT 101 potentiostat and the following: a Au disk working electrode ($A$ = 0.07 cm$^2$, Metrohm), a Pt auxiliary electrode (Metrohm), and a Ag/AgCl reference electrode (3 M NaCl, Metrohm, 0.222 V vs NHE at 20 °C). Solid samples of the complex were dissolved in small amounts of MeCN, which were then added to a larger volume of the respective aqueous buffer to yield a 1 mM solution. The ionic strength of the solution was adjusted by the addition of $LiClO_4$ to achieve a concentration of 0.1 M. All solutions were degassed with $N_2$ before measurement. All experiments were performed under $N_2$.

**Potentiometric Titration.** Potentiometric titration was performed on a Metrohm 702 SM Titrino in a jacketed, airtight glass titration cell equipped with a pH glass electrode (Metrohm, 3 M NaCl), an inlet and an outlet for $N_2$, and a graduated 10 mL microburet (Metrohm). The pH electrode was calibrated before measurement using commercially available standard buffer solutions (pH 4.0, 7.0, and 10.0). For titration, a 1 mM solution of the complex and a carbonate-free 0.05 M solution of NaOH were used. Sodium perchlorate was added to adjust the ionic strength of the solutions to 0.1 M. All solutions were degassed before use, and a nitrogen atmosphere was maintained during the experiment. The temperature was kept constant at 21 °C by a thermostat. Data analysis was performed using the software TITFIT.[18]

**Water Exchange: $^{17}O$ NMR Measurements.** $^{17}O$ NMR spectra were recorded on a Bruker AVANCE DRX 400WB spectrometer equipped with a spectrospin superconducting widebore magnet operating at a resonance frequency of 54.24 MHz at a magnetic induction of 9.4 T. The measurements at atmospheric pressure were performed with a commercial 5 mm Bruker broadband probe thermostated with a Bruker B-VT 3000 variable temperature unit. Relaxation rates were measured for both the paramagnetic solutions and metal-free aqueous buffer solutions. The line widths at half-height of the signal were determined by a deconvolution procedure on the real part of the Fourier transformed spectra with a Lorentzian shape function in the data analysis module of Bruker Topspin 1.3 software. Pressure-dependent measurements were done with a custom-made thermostated high-pressure probe.[19] The sample was measured in a standard 5 mm NMR tube cut to a length of 50 mm. To enable pressure transmittance to the solution, the NMR tube was closed with a moveable Macor piston. The advantage of this method is that oxygen-sensitive samples can be easily placed in the NMR tube and sealed with the Macor piston under an argon atmosphere. This facilitates subsequent transfer of the sample to the high-pressure probe. The pressure was applied to the high-pressure probe via a perfluorinated hydrocarbon (hexafluoropropylene oxide, Hostinert 175, Hoechst) and measured by a VDO gauge with an accuracy of ±1%. Temperature was adjusted with circulating, thermostated water (Colora thermostat WK 16) to ±0.1 K of the desired value and monitored before each measurement with an internal Pt-resistance thermometer with an accuracy of ±0.2 K. Enriched (10%) $^{17}O$-labeled water (D-Chem Ltd. Tel Aviv, Israel) was used for the $^{17}O$ NMR water exchange experiments. Samples were prepared by dissolving solid $[(L^{OH})Mn^{II}(MeCN)](ClO_4)_2$ in MeCN and refilling the sample with degassed buffer solution to get a 5 mM complex solution (containing 10% MeCN). To this solution, 10%-enriched $^{17}O$-labeled water was added, and the resultant solution was transferred to a NMR tube. For measurements at pH 7.4, 60 mM HEPES (4-(2-hydroxyethyl)-1-piperazineethanesulfonic acid) buffer was used since it shows a $pK_a$ value that is almost temperature- and pressure-independent. A detailed description of the experiments at pH 4.8 and general data treatment can be found in the Supporting Information (SI).

**EPR and Magnetic Measurements.** Methods for the EPR and magnetic measurements are outlined in the SI.

**X-ray Crystallography.** The intensity data for complexes were collected with an Agilent Technologies SuperNova, Dual, AtlasS2 diffractometer. The crystal of compound $[(L^{O^-})Mn^{II}](ClO_4)·1.5H_2O$ was a nonmerohedral twin. The twin law, relating the two twin components, was determined by CrysAlis[Pro 20] as (1.0003, 0.0014, 0.0009/−0.0010, −1.0000, 0.0007/−0.9849, −0.0021, −1.0011). Using Olex2,[21] the structure was solved by direct methods (ShelXT)[22] and refined with ShelXL[23] using least squares minimization. The fractional contribution of the minor twin component was refined to 0.4614(10). All non-hydrogen atoms were refined anisotropically. Most of the hydrogen atoms have been placed on calculated positions and were refined isotropically in a riding model. The positions of the hydrogen atoms of the three water molecules were located by difference Fourier synthesis and refined with an isotropic thermal parameter 1.5 times that of the attached oxygen atom.

CCDC 1496504 contains the supplementary crystallographic data for $[(L^{O^-})Mn^{II}](ClO_4)·1.5H_2O$. These data can be obtained free of charge from The Cambridge Crystallographic Data Centre via www.ccdc.cam.ac.uk/data_request/cif. (For X-ray crystallography of $[(L^{OH})Mn^{II}(OAc)](ClO_4)·nH_2O$ see SI.)

**Quantum Chemical Methods.** Density functional theory calculations were performed using the combination of exchange and correlation PW91-functionals;[24−26] this treatment yielded results comparable to those obtained with hybrid functional B3LYP[27−29] calculations. The performances of these functionals are well-documented.[30,31] In all cases, we applied the def2svp basis set.[32,33] For the PW91 calculations, the density fitting approach was applied.[34,35] All structures were characterized as local minima by computation of vibrational frequencies, and the stability of the wave function was successfully tested. The Gaussian 09 suite of programs was used.[36]

## ■ RESULTS AND DISCUSSION

**Speciation of $[(L^{OH})Mn^{II}(solv)](ClO_4)_2$ (1) in Aqueous (An)aerobic Solutions at Different pH Values: Potentiometric Titration, $^{17}O$ NMR Water Exchange Measurements, X-ray Structures, and CSI-Mass Spectrometry.** The $[(L^{OH})Mn^{II}(MeCN)](ClO_4)_2$ (1) complex was previously studied in organic solvents, and the structure of a species crystallized from MeCN solution was reported.[11,12] To better understand the behavior of 1 in aqueous solutions, we investigated the protonation state of the $L^{OH}$ ligand, the number and protonation states of coordinated water molecules, and the overall coordination number of the $Mn^{II}$ center as functions of pH. Analysis of potentiometric titration (see Figure 1, Table 1) suggests the existence of four $Mn^{II}$ species from pH



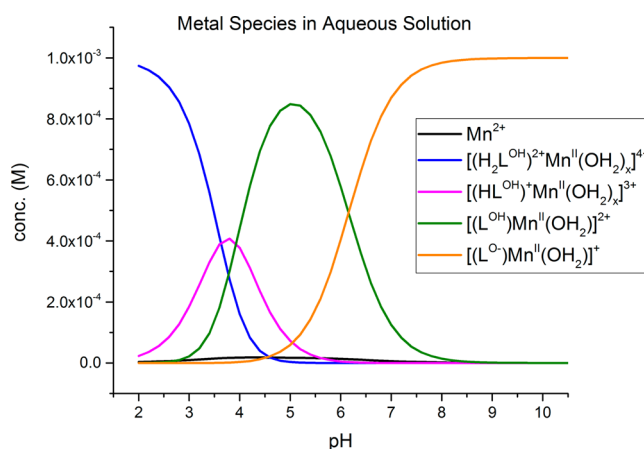**Figure 1.** Species distribution of $[(L^{OH})Mn^{II}(solv)](ClO_4)_2$ (1) in aqueous solution at 21 °C.

2 to 10; these correspond to the blue, pink, green, and orange curves in Figure 1. The observed acid−base, coordination, and redox equilibria (vide infra) are summarized in Scheme 1. Water exchange experiments were monitored by $^{17}O$ NMR at pH 4.8 and 7.4; the titration data suggest that a single species accounts for over 80% of the $Mn^{II}$ at these points. Additional CSI-MS experiments were performed to better understand the species distribution.

Since the reactivity studies of the species present in solution at pH >6 are of higher biological relevance, we will further focus on the speciation of 1 under these experimental conditions. Characterization of the species at pH <6 is provided in the SI.

**Table 1. pMn Values, Stability Constant, and p$K_a$ Values for the Ligand and Complex 1**

| | |
|---|---|
| $pK_{L1}{}^a$ | 4.11 |
| $pK_{L2}{}^a$ | 10.01 |
| $pK_a([(H_2L^{OH})^{2+}Mn^{II}]^{4+})^b$ | 3.63 |
| $pK_a([(HL^{OH})^{+}Mn^{II}]^{3+})^c$ | 3.93 |
| $pK_a([(L^{OH})Mn^{II}]^{2+})^d$ | 6.16 |
| $\log K([(L^{OH})Mn]^{2+})^e$ | 6.51 |
| pMn $(7.4)^f$ | 5.40 |

$^a$Ligand p$K_a$ values related to the (de)protonation of the free ligand (protonated pyridine and phenol groups, respectively), $K_{L1} = [L^{OH}][H^+]/[(HL^{OH})^+]$, $K_{L2} = [L^{O-}][H^+]/[L^{OH}]$. $^bK_a([(H_2L^{OH})^{2+}Mn^{II}]^{4+}) = [[(HL^{OH})^+Mn^{II}]^{3+}][H^+]/[[(H_2L^{OH})^{2+}Mn^{II}]^{4+}]$, related to a protonated pyridine group in the complex. $^cK_a([(HL^{OH})^+Mn^{II}]^{3+}) = [[(L^{OH})Mn^{II}]^{2+}][H^+]/[[(HL^{OH})^+Mn^{II}]^{3+}]$, related to a protonated pyridine group in the complex. $^dK_a([(L^{OH})Mn^{II}]^{2+}) = [[(L^{O-})Mn^{II}]^+][H^+]/[[(L^{OH})-Mn^{II}]^{2+}]$, related to the deprotonation of the phenol group in the complex. $^eK([(L^{OH})Mn^{II}]^{2+}) = [[(L^{OH})Mn^{II}]^{2+}]/[Mn^{2+}][L^{OH}]$. $^f$pMn $= -\log [Mn^{2+}]_{free}$ calculated for [complex] = 1 mM, $T = 21$ °C, pH 7.4.

At pH values above 6, the phenol in the $L^{OH}$ ligand is deprotonated (Scheme 1 and Figure 1). The p$K_a$ value obtained for coordinated phenol is 6.16 (Table 1), which is similar to values measured for other $Mn^{II}$–phenol complexes.[37]

Temperature- and pressure-dependent water exchange experiments (Figure 2 and Table 2) show the exchange of one water molecule. However, the water exchange process is one order of magnitude faster than at pH 4.8, where the hexacoordinate species with one aqua ligand and noncoordinated protonated phenol group exists (Scheme 1; for details see the SI). The mechanism changes its character from an associative to a dissociative one, which is best demonstrated by the positive activation volume (Table 2). These results can be explained by the coordination of the phenolate anion and the existence of a seven-coordinate structure in the ground state, with the singly deprotonated $L^{O-}$ ligand providing six donor atoms in addition to the one from the aqua ligand. As previously mentioned, water exchange involving seven-coordinate $Mn^{II}$ centers usually proceeds through $I_d$ mechanisms, which display $\Delta V^{\ddagger}$ values between approximately +3 and +5 cm$^3$ mol$^{-1}$.[38−41] The measured $\Delta V^{\ddagger}$ of +8.1 cm$^3$ mol$^{-1}$ for 1 at pH 7.4 is significantly more positive (Table 2), and the fast exchange rate of $1.3 \times 10^8$ s$^{-1}$ at 298 K suggests an additional labilization effect. Such fast water exchange on seven-coordinate $Mn^{II}$ has only been observed for overall negatively charged complexes with polyanionic ligands, such as EDTA.[39−41] Thus, both the volume of activation and the rate constant indicate the possible agency of a pure dissociative (D) mechanism, which has been unknown for ligand exchange processes involving $Mn^{II}$ species. A D mechanism would imply the existence of a six-coordinate

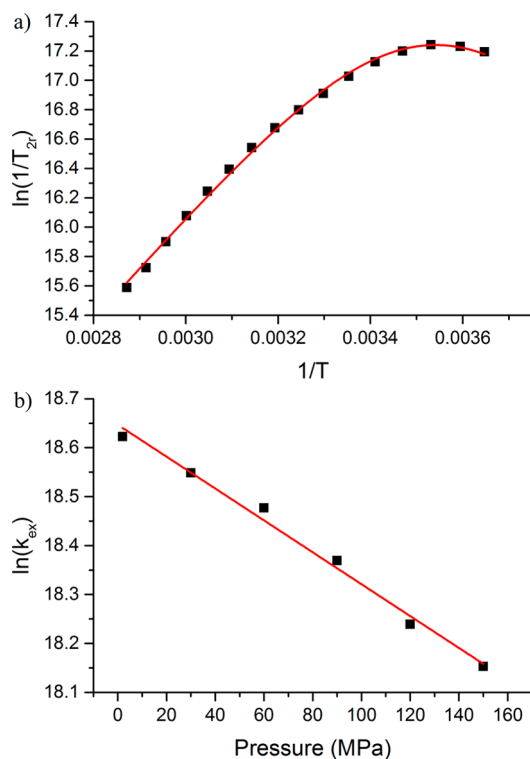**Scheme 1. Species Involved in Acid−Base, Coordination, and Redox Equilibria**
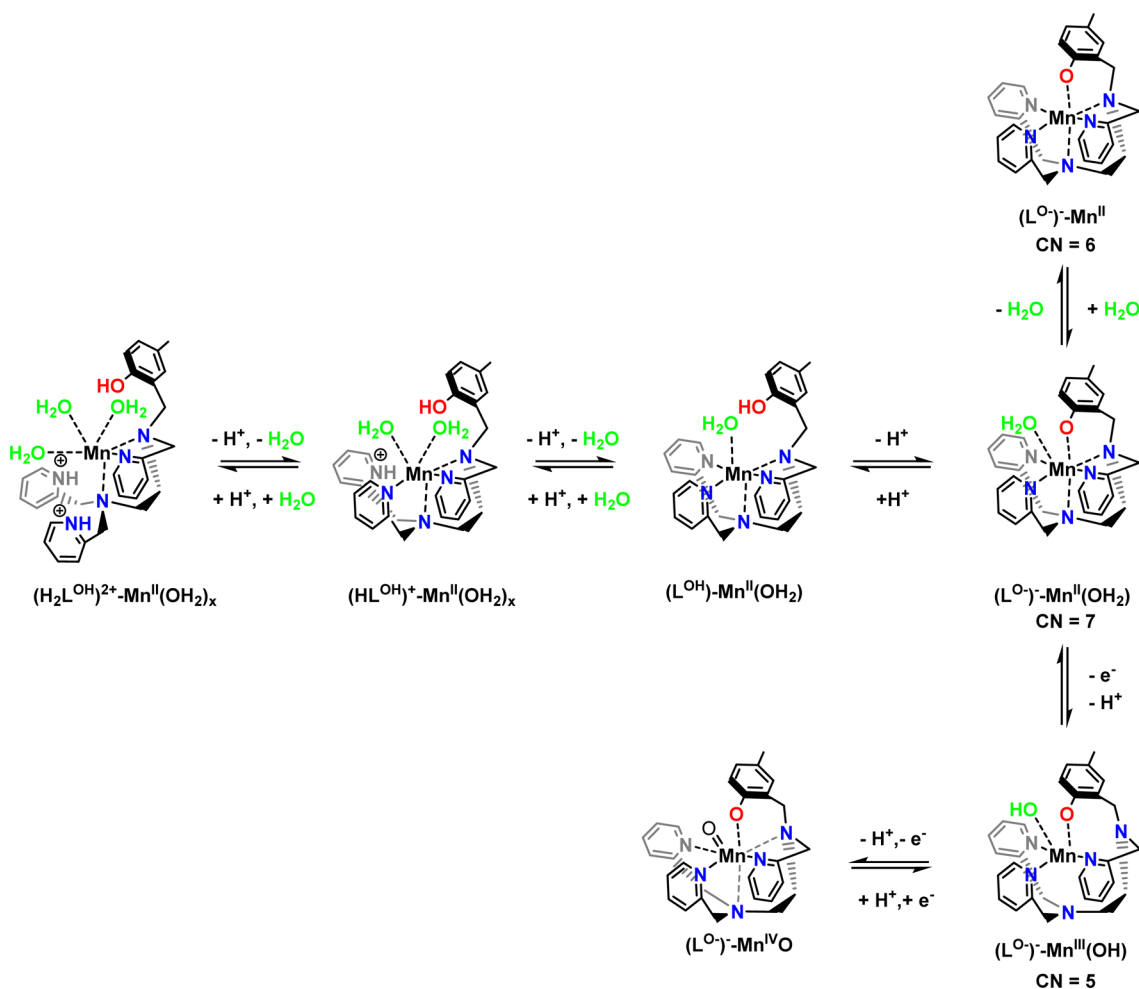
**Figure 2.** (a) Temperature dependence of the reduced transverse relaxation rate ($\ln(1/T_{2r})$) for the $[(L^{O-})Mn^{II}(OH_2)]^+$ complex at pH 7.4 (see eqs S4, S7, and S8 in the SI). (b) Pressure dependence of $\ln(k_{ex})$ at pH 7.4 and 298 K (see eq S6 in the SI).

intermediate with no bound water molecule. We crystallized this species from a neutral aqueous solution (see Figure 3). The $Mn^{II}$ center is coordinated in a distorted octahedral environment by the phenolate oxygen and the five nitrogen donors from the $L^{O-}$ ligand. The distorted geometry leaves a quite large gap between N4, N5, and O1 for the coordination of the aqua ligand during the water exchange process (see Figure 3 and Table 3). As in the structure obtained from MeCN,[11] the O-donor from the polydentate ligand participates in hydrogen bond interactions with outer-sphere water molecules.

The Mn−O bond in $[(L^{O-})Mn^{II}]^+$ is much shorter (2.037 Å) than that in the crystal structure of $[(L^{OH})Mn^{II}(MeCN)]^{2+}$, which contains a neutral phenol group (Mn−O = 2.367 Å).[11] The contraction of the Mn−O bond provides strong evidence for the assignment of a deprotonated phenol group in the $[(L^{O-})Mn^{II}]^+$ structure. It should be mentioned that the phenolate anion in $[(L^{O-})Mn^{II}]^+$ is anticipated to coordinate more strongly to $Mn^{II}$ than carboxylate groups, based on the shorter Mn−O distance in **1** compared to $Mn^{II}$ complexes that contain one monodentate carboxylate (average Mn−O distance: $2.18 \pm 0.07$ Å).[42] In the $Mn^{II}$ complexes of highly

negatively charged polydentate ligands, the Mn−O$_{carboxylate}$ bond distances were found to be 2.161 and 2.1809 Å for $[(H_21,2\text{-pdta})Mn^{II}(OH_2)]$ and $[(edta)Mn^{II}(OH_2)]^{2-}$, respectively.[43,44] Complexes with EDTA derivatives have been documented to undergo water exchange through $I_d$ mechanisms.[40] The greater strength of the Mn−O$_{phenolate}$ bond may necessitate a D, rather than an $I_d$, mechanism for water exchange for the seven-coordinate $[(L^{O-})Mn^{II}(OH_2)]^+$. The strong coordination of the phenolate anion probably plays a role in the labilization of the aqua ligand, enabling the isolation of the non-water-bound six-coordinate intermediate predicted by the D mechanism.

The deprotonated phenol interacts via hydrogen bonds with a water molecule that is in close proximity to the vacant coordination site on $Mn^{II}$ and is part of a hydrogen bond network that involves two additional water molecules and the coordinated phenolate of a second complex unit (see Figure 3). The hydrogen bond network can assist in rapid water exchange and formation of the six-coordinate intermediate that is in fast equilibrium with the seven-coordinate species. The six-coordinate $[(L^{O-})Mn^{II}]^+$ form has also been detected by CSI-MS ($m/z = 507.1815$) as the main species in solution at pH 7.4 (see Figure S12, SI). The EPR studies of the $[(tpen)Mn^{II}]^{2+}$ complex suggested that it is structurally heterogeneous in frozen MeCN solution.[2] Our results lead us to believe that a seven−six-coordination equilibrium may be operable for this system as well.

**Electrochemistry.** Cyclic voltammetry measurements demonstrate that the redox behavior of **1** is highly dependent on pH. Above pH 6 (e.g., pH 6.5 in Figure 4), one clear oxidation (0.546 V vs Ag/AgCl) and one reduction (0.386 V vs Ag/AgCl) signal appear. The peak separation of 160 mV is consistent with a quasi-reversible redox process, which we attribute to the subsequent deprotonation of a bound water molecule upon oxidation of $Mn^{II}$ to $Mn^{III}$.[2] There is a linear correlation between $E_{1/2}$ and pH (Figure S4, Table S4, SI), with a slope that is consistent with the transfer of one proton per electron, corresponding to the $[(L^{O-})Mn^{II}(OH_2)]^+/[(L^{O-})Mn^{III}(OH^-)]^+$ couple. At lower pH, the $Mn^{II}$ could not be oxidized. The inability to deprotonate the phenol group and the aqua ligand under these conditions precludes the stabilization of a $Mn^{III}$ species. At more positive potentials (higher than 0.5 V; see Figure S5, SI), an additional oxidation signal becomes clearly observable, which also shifts to lower potentials and becomes more prominent by increasing the pH; at the same time, the reduction signal almost disappears by scanning toward cathodic potentials.

This additional process can be assigned to the formation of a $Mn^{IV}$-oxo species. The high reactivity associated with $Mn^{IV}$-oxo species[45−47] provides an explanation for the disappearance of the reduction signal and our inability to observe it even with

**Table 2. Activation Parameters for the Water Exchange on Complex 1 {six-coordinate $[(L^{OH})Mn^{II}(OH_2)]^{2+}$ and seven-coordinate $[(L^{O-})Mn^{II}(OH_2)]^+$} Depending on pH**

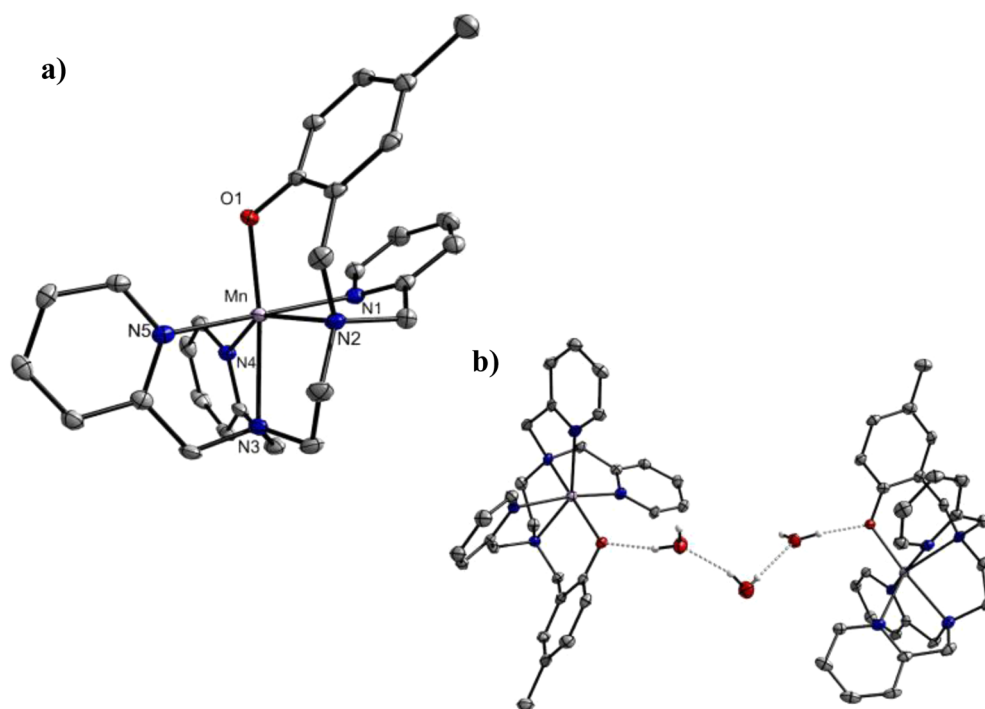|  | pH 4.8, $[(L^{OH})Mn^{II}(OH_2)]^{2+}$ | pH 7.4, $[(L^{O-})Mn^{II}(OH_2)]^+$ |
|---|---|---|
| $nH_2O$ | 1 | 1 |
| $k_{ex}^{298}$ (s$^{-1}$) | $1.9 \times 10^7$ | $1.3 \times 10^8$ |
| $\Delta H^{\ddagger}$ (kJ mol$^{-1}$) | $26.4 \pm 0.2$ | $26.6 \pm 0.5$ |
| $\Delta S^{\ddagger}$ (J mol$^{-1}$ K$^{-1}$) | $-17.0 \pm 0.7$ | $-0.65 \pm 1.68$ |
| $\Delta V^{\ddagger}$ (cm$^3$ mol$^{-1}$) | $-10.9 \pm 0.4$ | $+8.1 \pm 0.4$ |

**Figure 3.** Molecular structure of the cation of $[(L^{O-})Mn^{II}](ClO_4)\cdot 1.5H_2O$ (a) and two symmetry-independent $[(L^{O-})Mn^{II}]^+$ units bridged by a chain of three molecules of water (b). The displacement ellipsoids represent a probability of 50%; counterion, solvent molecules, and hydrogen atoms are omitted for clarity.

**Table 3. Selected Bond Lengths and Angles from the Structure of $[(L^{O-})Mn^{II}](ClO_4)\cdot 1.5H_2O$**

| bond | distance (Å) | bond | angle (deg) | bond | angle (deg) |
|---|---|---|---|---|---|
| N1−Mn1 | 2.311(3) | N1−Mn1−N2 | 74.61(9) | N2−Mn1−O1 | 91.13(8) |
| N2−Mn1 | 2.270(2) | N1−Mn1−N3 | 104.26(9) | N3−Mn1−N4 | 74.50(9) |
| N3−Mn1 | 2.321(2) | N1−Mn1−N4 | 92.07(9) | N3−Mn1−N5 | 75.11(9) |
| N4−Mn1 | 2.194(2) | N1−Mn1−N5 | 171.80(9) | N3−Mn1−O1 | 162.76(1) |
| N5−Mn1 | 2.251(3) | N1−Mn1−O1 | 87.93(9) | N4−Mn1−N5 | 95.59(9) |
| O1−Mn1 | 2.037(6) | N2−Mn1−N3 | 80.66(9) | N4−Mn1−O1 | 117.87(9) |
| O1−C27 | 1.334(4) | N2−Mn1−N4 | 147.95(9) | N5−Mn1−O1 | 91.07(9) |
| | | N2−Mn1−N5 | 97.27(9) | | |

faster scan rates. The complex likely quickly reacts further prior to the reduction scan.

The species involved in the acid−base and redox equilibria are summarized in Scheme 1. Notably, the related seven-coordinate $[(tpen)Mn^{III}Cl]^{2+}/[(tpen)Mn^{II}Cl]^+$ redox couple, though studied in MeCN, exhibits a redox potential at a ca. 0.6 V more positive value ($E_{1/2}$ = 1.05 V vs SCE).[2] The second anodic process attributed to the formation of a $Mn^{IV}$ species could be detected only at −20 °C at a 1 V more positive potential (+1.85 V vs SCE) than that for **1**. The much lower redox potentials required for the generation of the $Mn^{III}$ and $Mn^{IV}$ species from **1** allow us to observe these oxidized species merely by dissolving the $Mn^{II}$ precursor in aerobic buffer solutions at pH >6 (the reactivity toward oxygen is discussed further below), whereas the oxidation of $[(tpen)Mn^{II}Cl]^+$ and other related $Mn^{II}$ complexes with pyridylamine ligands can only be achieved by either bulk electrolysis or the addition of a strong oxidizing agent, such as $H_2O_2$ or *m*CPBA.[2] This dichotomy vividly illustrates how a PCET mechanism can render a difficult redox event into a thermodynamically favorable process. Even though the structurally related $[(L^{O-})Mn^{II}(OH_2)]^+$ and $[(tpen)Mn^{II}Cl]^+$ complexes hold the same overall charge, which remains the predominant influence

on the $E_{1/2}$ values,[2] the oxidation of the water-bound complex **1** is much more thermodynamically favored. The differences between $[(L^{O-})Mn^{II}(OH_2)]^+$ and $[(tpen)Mn^{II}Cl]^+$ also illustrate the importance of water coordination as a means to facilitate PCET and thereby enable novel reactive pathways.

**SOD Activity.** The observed PCET redox behavior of the complex prompted us to investigate its activity toward oxygen species. Manganese complexes that exhibit the proper redox potentials and coordination equilibria have been found to be potent SOD mimetics,[38,39,48−51] imitating the function of the manganese cofactor in mitochondrial SOD that cycles between five- and six-coordinate geometries during catalysis.[15] Thus, we followed the reaction between the $[(L^{O-})Mn^{II}(OH_2)]^+/[(L^{O-})Mn^{II}]^+$ complex and superoxide by using an established direct stopped-flow assay in which a DMSO solution of $KO_2$ is rapidly mixed with an aqueous solution containing catalytic amounts of the complex.[17] The SOD activity was studied in three different aqueous solutions: 60 mM HEPES at pH 8.1, 60 mM HEPES at pH 7.4, and 50 mM phosphate buffer at pH 7.4. As anticipated, the reactions were rapid, and the superoxide vanishes via a first-order process. The rate law suggests catalytic decomposition of superoxide. Superoxide will degrade without a catalyst, but this reaction is second-order with respect to
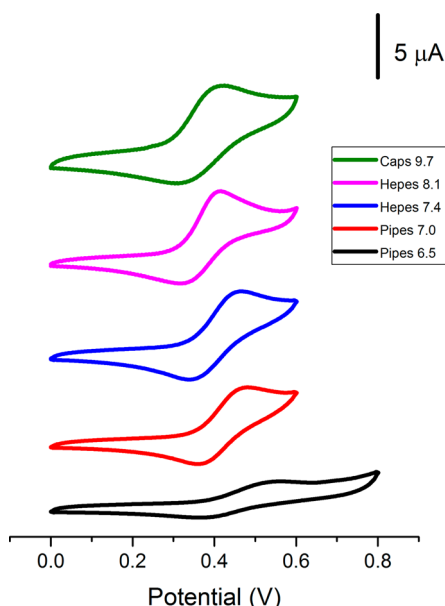
**Figure 4.** Cyclic voltammograms of $[(L^{O-})Mn^{II}(OH_2)]^+/[(L^{O-})-Mn^{III}/(OH^-)]^+$ in aqueous solution in relation to pH. [complex] = 1 mM, $[LiClO_4]$ = 100 mM, scan rate 0.1 V/s.

superoxide. The observed rate constants exhibit a linear dependence on the complex concentrations, and catalytic rate constants ($k_{cat}$) could be determined from the corresponding slopes [see Figure S6 (SI) and Table 4].

Previously, a chemiluminescent assay suggested that $[(L^{O-})-Mn^{II}]^+$ was an extremely effective superoxide scavenging agent at pH 8.[12] Despite this, the observed SOD activity reported here is in the lower range for characterized SOD mimetics, which have $k_{cat}$ values that span from $10^6$ to $10^9$ $M^{-1}$ $s^{-1}$.[17,52] This sort of discrepancy has precedence. The results obtained by indirect SOD assays often disagree with those from direct stopped-flow measurements, since side reactions interfere with the former.[17,49,53] As reported for different classes of SOD mimetics, the nature of the buffer also impacts the catalytic rate.[17] At pH 7.4, the complex degrades $O_2^{\bullet-}$ about twice as fast in HEPES than it does in phosphate buffer. The inhibitory effect of phosphate has previously been observed with pentaazamacrocyclic SOD mimetics and was believed to result from the competitive binding of hydrogen phosphate ($HPO_4^{2-}$) to the manganese center.[17]

**Reductive Activity toward Oxygen and Superoxide.** Besides SOD activity, the $Mn^{II}$ species is also capable of reducing oxygen. At pH >6, where the phenol group is deprotonated, the oxidation of the manganese center to $Mn^{III}$ becomes feasible in aerobic solutions. The $Mn^{III}$ complex can be further stabilized by deprotonation of the bound water (see Scheme 1), which yields the hydroxo species $[(L^{O-})-Mn^{III}(OH^-)]^+$. Above pH 6, the $[(L^{O-})Mn^{III}(OH^-)]^+$ could be detected in aerobic solutions by CSI-MS ($m/z$ = 524.1834;

Figure S13, SI). More basic conditions facilitate the oxidation of the $Mn^{II}$ in saturated oxygen solutions; under these conditions, the oxidation can be followed spectrophotometrically. A new UV/vis absorption band develops at 420 nm, a wavelength that is characteristic for $Mn^{III}$-related LMCT bands (Figure S7a, SI).[2,54,55] These compounds include $[(tpen)Mn^{III}Cl]^{2+}$, which coincidentally also features a UV/vis band at 420 nm, albeit in MeCN.[2] We observed the same UV/vis spectral features upon electrochemical generation of Mn(III) at 500 mV (vs Ag wire), which confirmed the characterization of the product of the reaction with oxygen (see SI material and Figure S7b).

One notable difference between $Mn^{II}$ and $Mn^{III}$ is that $Mn^{III}$ does not support seven-coordinate geometry.[56] Heptacoordinate $Mn^{III}$ of a capped–trigonal prism geometry was only reported in the solid state for the aforementioned $[(tpen)-Mn^{III}Cl]^{2+}$, which is structurally analogous to **1**.[2] However, in that structure, two Mn–N bonds are substantially elongated with average bond lengths of 2.47 Å, and it is questionable whether it retains its heptacoordinate geometry in solution.

Parallel computational studies revealed that the $[(L^{O-})-Mn^{III}(OH^-)]^+$ cation is more stable with a pentacoordinate geometry, since two of the Mn–N distances ($d$ = 2.81 and 2.63 Å) are inconsistent with Mn–N bonds (Figure 5a). This is again a consequence of the strong coordination of the phenolate and hydroxo groups; this induces additional labilization of the Mn–N bonds in comparison to the structure of $[(tpen)Mn^{III}Cl]^{2+}$, which has only one negatively charged donor atom, from the more weakly binding chlorido ligand.[2] By way of comparison, our calculated average Mn–O bond length of 1.88 Å (Table S5, SI) is identical to that experimentally observed by EXAFS measurements for a related Mn(III) complex with phenolate and hydroxo groups in the coordination sphere.[57]

Furthermore, in aerated complex solutions at neutral to slightly basic pH, the adducts of the complex with oxygen and its reduced species, respectively, could also be detected by CSI-MS in addition to $[(L^{O-})Mn^{III}(OH^-)]^+$ and $[(L^{O-})Mn^{IV}O]^+$ (see Figures S13 and S14, SI). One of the generated species has a peak at $m/z$ = 539.1703, which corresponds to either $[(L^{O-})Mn^{II}(O_2)]^+$ or its redox tautomer $[(L^{O-})Mn^{III}(O_2^{\bullet-})]^+$ (Figure S14, SI). Our DFT calculations support its assignment as a $Mn^{III}$-superoxo species [Figure 5b, Table S5 (SI)]. These show that coordination of $O_2$ to hexacoordinate $[(L^{O-})Mn^{II}]^+$ results in a weakened O–O bond. The 1.27 Å O–O bond distance is consistent with a metal-bound superoxide in an end-on binding mode (1.280 Å).[58] In addition, the shortening of the Mn–phenolate bond and the significant elongation of the bonds between the Mn and the two backbone amine nitrogens suggest the significant $Mn^{III}$ character of the metal center (Figure 5b).

The second new feature at $m/z$ = 540.1788 corresponds to either the protonated superoxide (perhydroxyl radical) or hydroperoxo adduct, i.e. $[(L^{O-})Mn^{II}(HO_2^{\bullet})]^+$ or $[(L^{O-})-Mn^{III}(HO_2^-)]^+$ (Figure S14, SI). The latter assignment is

**Table 4. Catalytic Rate Constants of the Reaction of 1 and 2 with Superoxide**

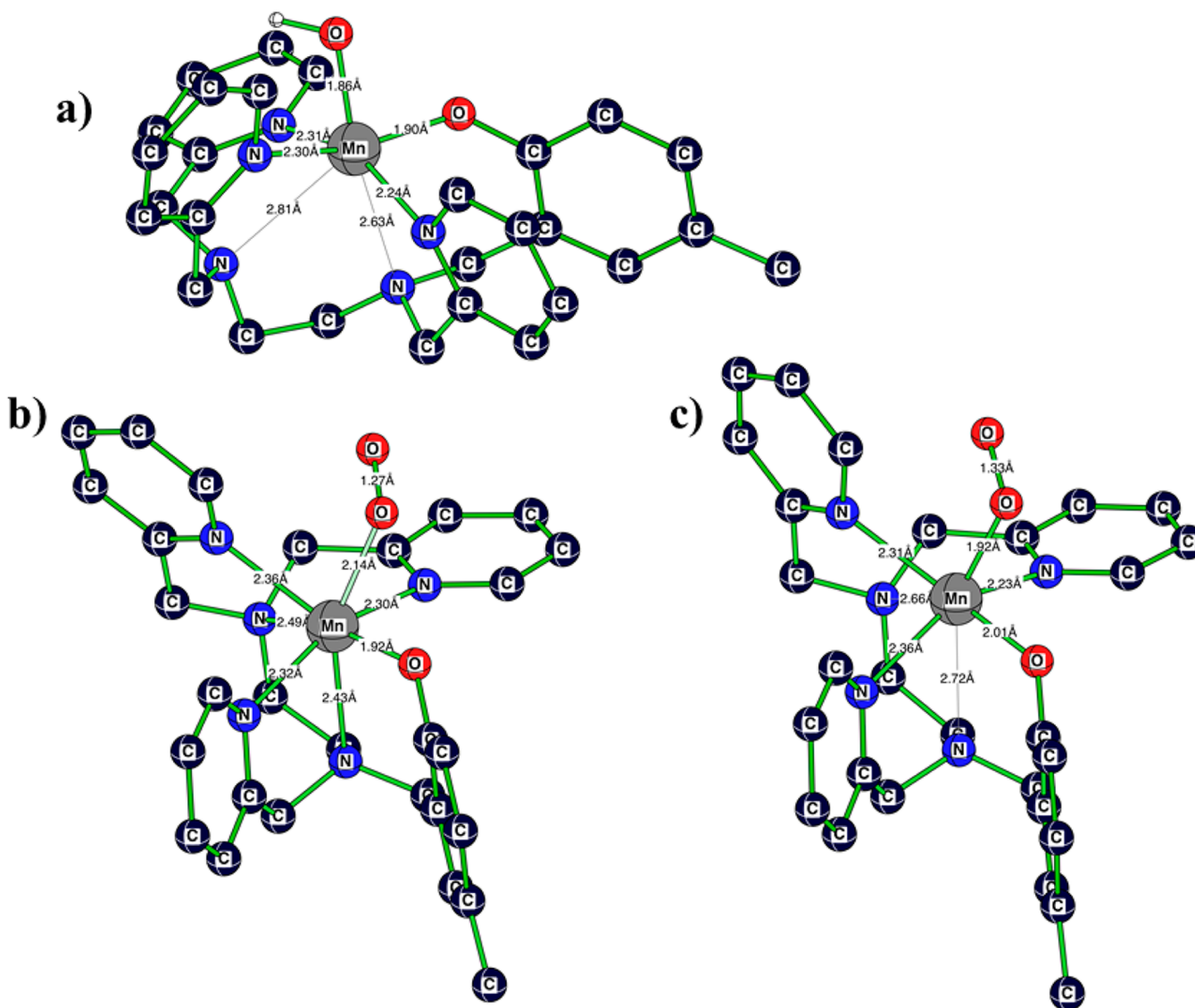| | $k_{cat}$ ($M^{-1}$ $s^{-1}$) | |
| --- | --- | --- |
| buffer, pH | $[(L^{O-})Mn^{II}]^+/[(L^{O-})Mn^{II}(OH_2)]^+$ (**1**) | $[(^{HO}L-L^{O-})Mn^{II}_2(OH_2)_x]^{3+}$ (**2**) |
| HEPES, 8.1 | $6.2 \pm 0.5 \times 10^5$ | $1.6 \pm 0.1 \times 10^6$ |
| HEPES, 7.4 | $3.6 \pm 0.1 \times 10^6$ | $5.1 \pm 0.3 \times 10^6$ |
| phosphate, 7.4 | $1.1 \pm 0.02 \times 10^6$ | $2.5 \pm 0.2 \times 10^6$ |

**Figure 5.** Calculated structures (UPW91PW91/def2svp) of (a) $[(L^{O-})Mn^{III}(OH^-)]^+$, (b) $[(L^{O-})Mn^{III}(O_2^{\bullet-})]^+$, and (c) $[(L^{O-})Mn^{III}(O_2^{2-})]$. The hydrogen atoms of the polydentate ligand were omitted for clarity.

more plausible, since the superoxide adduct of a $Mn^{II}$ complex with an analogous pentadentate ligand was proven to have $Mn^{III}$-peroxo character.[59] The existence of these species suggests that oxidation of the $Mn^{II}$ complex to $[(L^{O-})Mn^{IV}O]^+$ proceeds through oxygen binding to the six-coordinate $Mn^{II}$ center that triggers an inner-sphere electron transfer and superoxide generation. This we could also confirm by DFT calculations that demonstrate cleavage of the $Mn^{III}$–superoxo bond upon addition of a proton and release of $HO_2$ (Figure S8a, SI). The latter can bind to excess $Mn^{II}$ present in solution and undergoes an inner-sphere reduction to the corresponding hydroperoxo adduct $[(L^{O-})Mn^{III}(HO_2^-)]$, with subsequent homolytic cleavage of the O–O bond resulting in the $Mn^{IV}$-oxo species and the $OH^{\bullet}$ radical (red pathway in Scheme 2). We also probed the character of the $Mn^{II}$-superoxo adduct by DFT studies. As expected (see above), binding of superoxide to hexacoordinate $[(L^{O-})Mn^{II}]^+$ results in a structure that resembles that of a pentacoordinate end-on $Mn^{III}$-peroxo complex [Figure 5c, Table S5 (SI)] based on the Mn–N, Mn–phenolate, O–O, and Mn–$O_2$(unit) bond lengths. Addition of a proton leads to protonation of the distal peroxo

oxygen atom that is accompanied by elongation of the O–O bond and shortening of the Mn–O bond with negatively charged phenolate and vicinal oxygen (from the O–O moiety) atoms, respectively (Figure S8b, SI). This at least qualitatively explains a tendency toward O–O bond splitting and generation of the $Mn^{IV}$-oxo species and hydroxyl radical upon protonation of coordinated peroxide.

On the basis of the redox potential of **1**, an outer-sphere reduction of $O_2$ to $O_2^{\bullet-}$ by the $Mn^{II}$ form is thermodynamically unfavorable; therefore, an inner-sphere pathway, proceeding through the observed hexacoordinate $[(L^{O-})Mn^{II}]^+$ intermediate, that binds $O_2$ represents the only possible mechanism for its reduction.

We experimentally confirmed the generation of reactive oxygen species (ROS) by following of the oxidation of 2-nitro-5-thiobenzoate (TNB) to 5,5′-dithiobis(2-nitrobenzoic acid) (DTNB) spectrophotometrically, as well as by EPR measurements (for details see the SI).

On the basis of the observed manganese and reduced oxygen species, as well as their adducts, an overall mechanism for the oxygen/superoxide reduction by **1** is depicted in Scheme 2 (red

**Scheme 2. Overall Reaction Scheme, Which Links Outer Sphere, Inner Sphere, and Water Exchange Reactivity of $[(L^{O-})Mn^{II}]^+$ at pH >6**
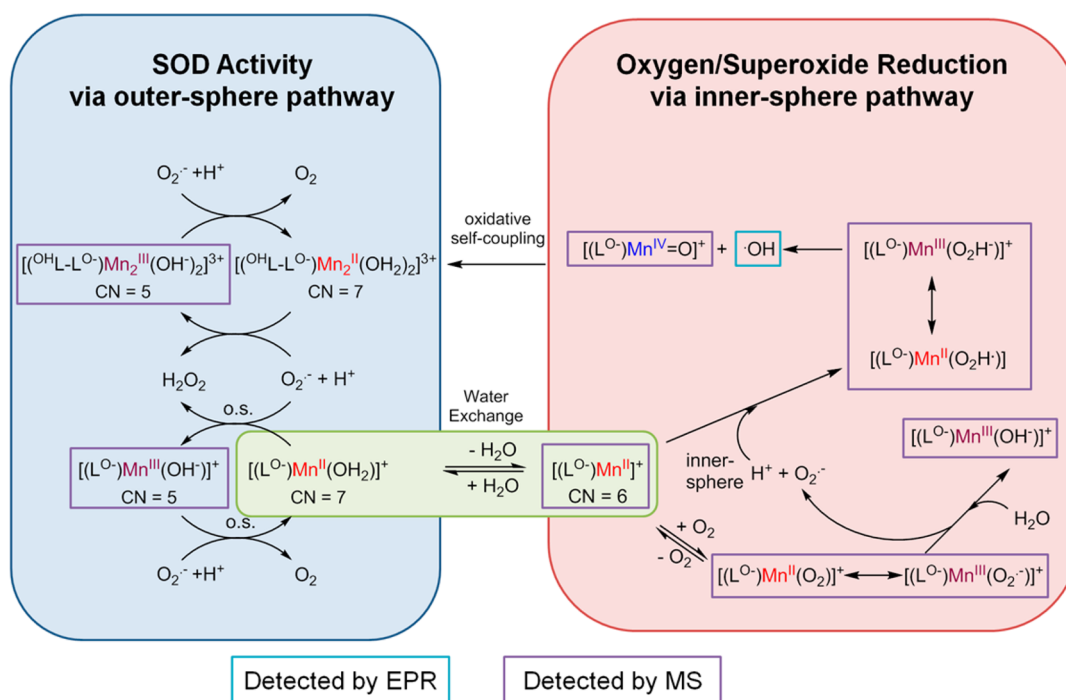


**Scheme 3. Oxidative Coupling of Two Molecules of $[(L^{O-})Mn^{II}]^+$ Induced by $[(L^{O-})Mn^{IV}O]$, $OH^\bullet$, or $H_2O_2$**
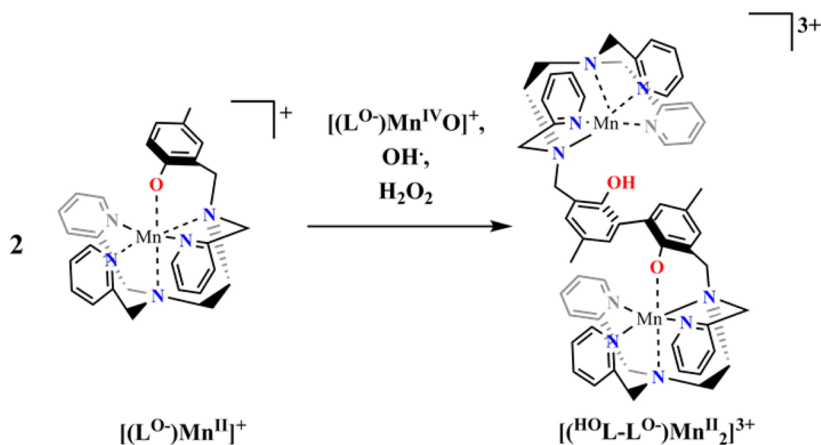


field). Importantly, the binding of superoxide to six-coordinate $Mn^{II}$ and its subsequent inner-sphere reduction does not seem to contribute to the superoxide dismutation path, since the decay of the corresponding $Mn^{III}$-hydroperoxo adduct yields a $Mn^{IV}$-oxo species and $OH^\bullet$, rather than the $Mn^{III}$ required to continue the SOD catalytic cycle (see above). Even more, we probed coordination of superoxide to the $Mn^{III}$ form of **1** that exists under our experimental conditions, i.e., pentacoordinate $[(L^{O-})Mn^{III}(OH)]^+$, by computational methods. However, superoxide did not show a tendency to bind to $[(L^{O-})Mn^{III}(OH^-)]^+$ at all, suggesting that repulsions between the negatively charged superoxide and phenolate, the steric bulk of the $L^{O-}$ ligand, and the lesser kinetic lability of $Mn^{III}$ [60] make $[(L^{O-})Mn^{III}(OH^-)]^+$ coordinatively saturated and inert toward substitution/addition reactions. All together, our results suggest that the SOD catalysis displayed by **1** is predominantly achieved through an outer-sphere mechanism that involves coordinationally saturated species: heptacoordinate $[(L^{O-})-$

$Mn^{II}(OH_2)]^+$ and pentacoordinate $[(L^{O-})Mn^{III}(OH^-)]^+$ (see blue field in Scheme 2). In comparison, manganese complexes with pentaazamacrocyclic ligands also exhibit equilibria between seven- and six-coordinate species, yet they possess significantly higher SOD activity, with $k_{cat}$ up to three orders of magnitude bigger than **1**, despite their having much more positive redox potentials that do not favor superoxide reduction.[49−51,61] The oxidized and reduced forms of these complexes, either six- and seven-coordinate $Mn^{II}$ ($[(L)-Mn^{II}(OH_2)]$ and $[(L)Mn^{II}(OH_2)_2]$) or six-coordinate $Mn^{III}$ ($[(L)Mn^{III}(OH_2)]$), possess at least one readily exchangeable water molecule in their coordination spheres.[39,61] Further, their pentagonal bipyramidal coordination environment with the neutral pentadentate ligand in the equatorial plane does not hinder the access of negatively charged substrate molecules to the metal center.[39,49−51,62] The ability of the pentaazamacro-cylic complexes to operate through an inner-sphere mechanism
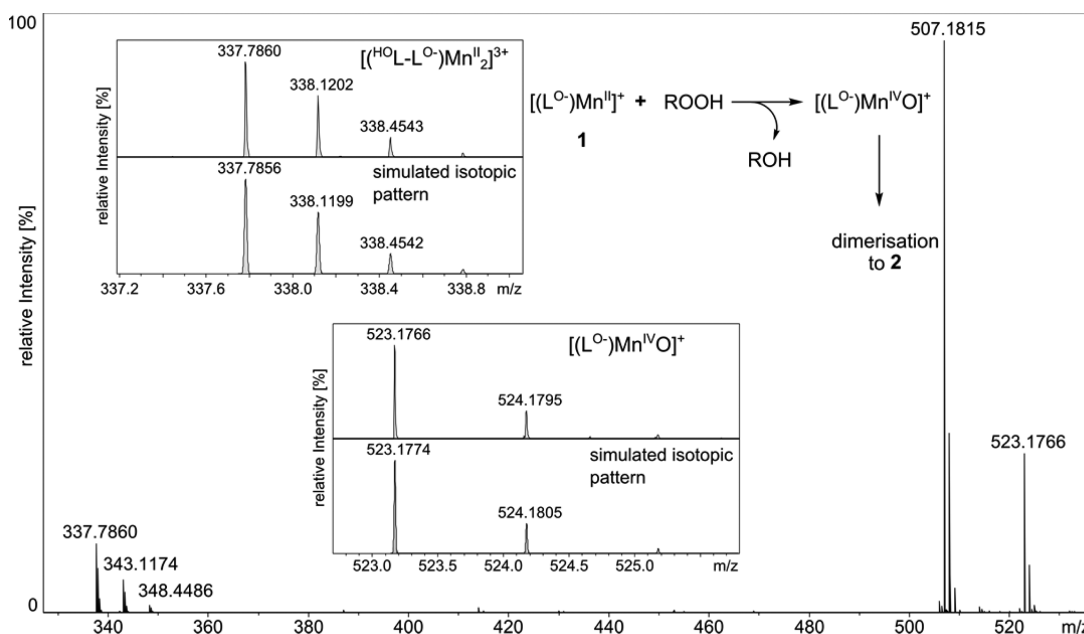
**Figure 6.** CSI-MS of a solution of **1** in acetonitrile mixed with *m*CPBA. Detection of $[(L^{O-})Mn^{II}]^+$ ($m/z = 507.1815$) in addition to $[(L^{O-})Mn^{IV}O]^+$ ($m/z = 523.1766$) and $[(^{HO}L-L^{O-})Mn^{II}_2]^{3+}$ ($m/z = 337.7860$).

compensates for their less favorable redox potentials and results in efficient catalysis.[49−51]

**Transformation into Binuclear Complex [(HOL–LO−)-MnII2]3+ (2) by ROS Prolongs SOD Catalysis (stability, magnetic properties, and SOD activity of 2).** The competition between outer-sphere SOD catalysis and inner-sphere reduction of oxygen and superoxide is determined by the equilibrium between the heptacoordinate $Mn^{II}$ complex and the hexacoordinate $Mn^{II}$ species that serves as the intermediate for water exchange (see green field in Scheme 2). The reaction with oxygen is slow, whereas the reaction with superoxide is rapid. Nonetheless, one would expect that the $OH^\bullet$ and $Mn^{IV}$-oxo species generated by the inner-sphere pathway would eventually result in oxidative degradation of the complex, as has been observed in MeCN for similar $Mn^{II}$ complexes,[63] and the concomitant loss of SOD activity.

One of our groups previously reported that the reaction between **1** and $H_2O_2$ results in oxidative coupling of the phenol groups from two different equivalents of **1**, yielding a stable binuclear $Mn^{II}$ complex **2** (see Scheme 3).[11] During this process, a transient color change from pale yellow to brown was observed and ascribed to the temporary oxidation of the manganese.[11] Reacting **1** with the less reactive organic peroxide *m*CPBA (see Figure 6, ROOH = *m*CPBA) instead of $H_2O_2$ in MeCN allowed us to observe both $Mn^{IV}$-oxo ($m/z = 523.1766$) and the binuclear species **2** ($[(^{-O}L-L^{OH})Mn^{II}_2]^{3+}$, $m/z = 337.7860$; Figure 6) by CSI-MS. These results suggest that the $Mn^{IV}$-oxo complex may be an intermediate for the formation of the binuclear species. Since the reaction between **1** and ROOH is not anticipated to result in generation of an organic radical (scheme in Figure 6), the $Mn^{IV}$-oxo species seems to be the oxidizing agent responsible for the oxidative coupling of the $L^{OH}$ ligand. MS analysis of the reaction mixture obtained after the catalytic decomposition of superoxide also revealed the formation of **2**. We currently speculate that both $Mn^{IV}$-oxo[45] and $OH^\bullet$, each of which is capable of hydrogen atom abstraction, contribute to the oxidative self-dimerization of the complex through the ligand phenol groups (see red field in

Scheme 2). In the oxidizing solutions, where generation of **2** was observed, we could also detect trace amounts of mono- and dihydroxylated forms $\{[(^{HO}L(OH)-L^{O-})Mn^{II}_2]^{3+}$, $m/z = 343.1174$ and $[(^{HO}L(OH)-(HO)L^{O-})Mn^{II}_2]^{3+}$, $m/z = 348.4486$; Figures 6 and S15 (SI)}, which feature one or two further hydroxylated phenol groups of ligand, respectively. The presence of this product is consistent with the agency of a $Mn^{IV}$-oxo intermediate; such species are known to activate aromatic C−H bonds.[45] The additional OH groups render the ligand environment around the Mn centers within the binuclear structure even more crowded.

We attempted to compare the stability of the mono- and binuclear analogues and measure the formation constant of **2** through a competitive binding assay with tpen. The tpen ligand had previously been found to remove the $Mn^{II}$ from **1**.[11] Even after adding four equiv of tpen to a solution of the binuclear complex **2** in a mixture of MeCN and MeOH, there was no evidence of its dissociation. No new resonances that could be assigned to the dimeric $^{HO}L-L^{OH}$ ligand appeared, as would be anticipated from its displacement from the highly paramagnetic $Mn^{II}$.[11] The results suggest that the stability of **2**, which is obtained upon interaction between reactive oxygen species and **1**, is superior to that of its mononuclear analogue **1**. By way of comparison, it was previously demonstrated that the binuclear structures of seven-coordinate $Mn^{II}$ SOD mimetics based on the pentaazamacrocyclic ligands provide higher complex stabilities than their corresponding mononuclear structures.[38]

In order to understand the overall mechanism behind the catalytic superoxide decomposition initially induced by **1**, we studied the SOD activity of pure **2** under the same experimental conditions. The obtained catalytic rate constants per manganese center are comparable to those observed for the mononuclear complex [see Table 4 and Figure S6 (SI)]. This suggests that there is no significant electronic communication between the two manganese centers within the binuclear complex[11] and that they behave independently as catalysts. A similar phenomenon was observed for binuclear analogues of the $Mn^{II}$ pentaazamacrocyclic SOD mimetics.[38]

The previously reported crystal structure of **2** obtained from MeCN showed that the two $Mn^{II}$ centers retain the same seven-coordinate geometry as the metal center in **1**.[11] One of the phenols is deprotonated and the seventh coordination site is occupied by the solvent molecule. In aqueous solution, the water molecules coordinated to **2** might be significantly more acidic than those in **1**, as has been observed in the case of mono- and binuclear pentaazamacrocyclic SOD mimetics.[38] This would stabilize dihydroxo $[(^{HO}L-L^{O-})Mn^{II}_2(OH^-)_2]^+$ species over the diaqua species. This difference is significant, since hydroxide anions should be more difficult to displace from the metal ions than water molecules. Attempts to determine the $pK_a$ values, stability constants, and rate constants for water exchange of **2** failed due to the low water solubility of the compound.

To further assess the electronic independence of the $Mn^{II}$ centers in **2**, we performed variable temperature magnetic susceptibility measurements. The magnetic data for **2** are consistent with the notion that the $Mn^{II}$ centers are essentially separate entities, arising from the lack of an obvious orbital pathway for communication of spin information between the ions (for details, see the SI).

On the basis of the collective obtained results, a proposed mechanism that accounts for the observed interactions of **1** with superoxide and oxygen is summarized in Scheme 2. Once the binuclear complex **2** is formed, it probably also contributes to the SOD catalytic cycle by an outer-sphere mechanism (Scheme 2). This would be in agreement with the fact that the electronic nature of the manganese centers is the same in **1** and **2** and should therefore result in similar outer-sphere catalytic rates. A preference for the outer-sphere SOD mechanism results from the fact that (i) the $Mn^{III}$ forms both in **1** and **2** are inert toward superoxide binding (see above), (ii) the binding of negatively charged superoxide to two $Mn^{II}$ centers in the binuclear structure might not be sterically/electrostatically favored, (iii) the binuclear $Mn^{II}$ form might be more acidic than the mononuclear one and would consequently exist in a form, $[(^{HO}L-L^{O-})Mn^{II}_2(OH^-)_2]^+$, with a less labile exogenous ligand that would hinder the IS mechanism, and (iv) the binding of superoxide to six-coordinate mononuclear $Mn^{II}$ leads to reactions that generate $Mn^{IV}$-oxo and $OH^\bullet$, inducing the formation of the binuclear complex that continues to superoxide dismutation via an OS mechanism (Scheme 2).

## ■ CONCLUSION

The $L^{OH}$ complex with $Mn^{II}$ is capable of both outer-sphere and inner-sphere reactions with superoxide, with the coordination of water determining which pathway is followed. The heptacoordinate complex $[(L^{O-})Mn^{II}(OH_2)]$ engages in superoxide dismutation, whereas the hexacoordinate species $[(L^{O-})Mn^{II}]^+$ only reduces superoxide. Enzymatic systems and some efficient SOD mimetics rely on the operation of both inner-sphere and PCET processes for the rapid catalysis of superoxide degradation,[49−51] whereas the latter can also assist in operation of an OS electron transfer mechanism. Although OS PCET is provided by **1**, the IS mechanism leads to superoxide reduction side reactivity. In $[(L^{O-})Mn^{III}(OH_2)]$, the bound water molecule supports PCET by lowering the $Mn^{III}/Mn^{II}$ and $Mn^{IV}/Mn^{III}$ redox potentials enough to allow efficient OS SOD catalysis. The importance of water coordination is nicely illustrated by the fact that $[(L^{O-})Mn^{II}(OH_2)]^+$ can be oxidized to $Mn^{III}$ and $Mn^{IV}$ at potentials that are at least 0.6 and 1 V, respectively, less positive than those required for the oxidation

of the structurally related $[(tpen)Mn^{II}(Cl)]^+$, which has the same overall charge but lacks an inner-sphere water. The lowering of these redox potentials also facilitates the generation of a $Mn^{IV}$-oxo species, which contributes to the superoxide and oxygen reduction ability of the complex. Similar effects would be anticipated for the active sites of other oxido-reductase enzymes; these are typically highly accessible to water molecules.

The operation of SOD catalysis according to an IS mechanism, cannot be provided by **1**. In order for an IS mechanism to proceed, either a vacant coordination site or a labile ligand in the coordination sphere of both $Mn^{II}$ and $Mn^{III}$ forms is required. The MnSOD enzyme cycles through five-coordinate $Mn^{II}$ and $Mn^{III}$ trigonal bipyramidal forms that are sterically uncongested enough to accommodate superoxide as the sixth ligand in the equatorial plane.[64] Although the $Mn^{III}$ center in $[(L^{O-})Mn^{III}(OH^-)]^+$ is also pentacoordinate with three neutral nitrogen and two negatively charged oxygen donor atoms as in the MnSOD enzyme, its distorted square pyramidal structure and the diamine backbone of the ligand block the access of potential sixth ligands. The axial position is therefore inaccessible and is not capable of binding superoxide. In addition, the strong coordination of phenolate hinders entrance of a third negatively charged ligand into the coordination sphere of $[(L^{O-})Mn^{III}(OH^-)]^+$. In the case of efficient seven-coordinate pentaazamacrocyclic SOD mimetics, the equatorially positioned pentadentate ligands do not exert any steric hindrance for the entry of additional substituents;[39,49−51,62] consequently, both their oxidized and reduced forms possess at least one labile aqua ligand, enabling IS mechanisms. The pentadentate ligands for these complexes are neutral; this results in more positive overall complex charges and much higher redox potentials. The higher potentials preclude efficient OS SOD catalysis. Nonetheless, these compounds still exhibit remarkable SOD activity (higher than that of **1**) with catalytic rate constants comparable with those of the enzymes ($k_{cat} \sim 10^9$ $M^{-1}$ $s^{-1}$ for MnSOD,[65] $1.60 \times 10^9$ $M^{-1}$ $s^{-1}$ for M40401[52]). The results here demonstrate how the operation of an IS mechanism can assist SOD catalysis.

Different from the $Mn^{III}$ form of **1**, its $Mn^{II}$ hexacoordinate form is capable of reducing oxygen and superoxide by the IS mechanism. Importantly, reduction of oxygen to superoxide, which is formally the reverse of what proceeds within the SOD cycle, would not be feasible without coordination of oxygen. Upon binding of oxygen to $Mn^{II}$, the redox potential of the $O_2/O_2^-$ couple shifts to values higher than that for the corresponding $Mn^{III}/Mn^{II}$ couple, thus enabling IS reduction of $O_2$.[49,50]

One substantial difference between the aforementioned pentaazamacrocyclic SOD mimetics and **1** and its binuclear form **2** is that the latter two complexes have more sterically crowded metal centers, with negatively charged phenolate groups close to the only accessible coordination site for an entering substrate. Thus, superoxide can only bind to $Mn^{II}$ through the six-coordinate water-free intermediate. The obtained $Mn^{III}$-hydroperoxo intermediate undergoes homolytic O−O cleavage instead of being protonated to release $H_2O_2$. A byproduct of the O−O cleavage is a $Mn^{IV}$-oxo species that reacts with another equivalent of Mn complex to form **2**. The low redox potential for the $Mn^{IV}/Mn^{III}$ couple favors such reactivity. Outside of Mn−corrole systems,[66] this is the only known example of the involvement of a $Mn^{IV}$-oxo species in SOD catalysis, albeit through the separate superoxide/oxygen

reduction path. Another key difference between the pentaaza-macrocyclic SOD mimetics and **1** is the coordination of the $Mn^{III}$ members of the main catalytic cycle. In the former, the $Mn^{III}$ forms are proposed to be six-coordinate with neutral pentadentate and aqua ligands;[52] conversely, the $Mn^{III}$ form of **1**, $[(L^{O-})Mn^{III}(OH^-)]^+$, is pentacoordinate, with the bulky and negatively charged $L^{O-}$ and a $OH^-$ ligand that is substitutionally inert relative to the aforementioned aqua ligands.

The high redox potentials of the pentaazamacrocyclic SOD mimetics inhibit the formation of high-valent $Mn^{IV}$ or $Mn^V$ species, representing a means to defend the active site against inadvertent oxidative damage. Study of the solution properties and redox reactivity of **1**, conversely, reveals that the compound retains its SOD activity via its unique ability to self-scavenge the $OH^\bullet$ and $Mn^{IV}$-oxo species that are generated through inner-sphere reactions between the complex and oxygen, superoxide, and/or hydrogen peroxide. These side products convert the complex into what appears to be a more stable binuclear form, **2**, that maintains both the same coordination geometry around the $Mn^{II}$ centers and the same catalytic activity. The SOD activity of **2** appears to operate through fundamentally the same OS mechanism as **1**. The channeling of these oxidants toward a reaction that produces a catalytic species that is less susceptible to side reactivity represents an alternative mechanistic strategy to both defend a catalyst against oxidative damage and prolong catalysis. This strategy could potentially be applied to prolong the catalysis of other oxidation reactions, such as non-heme iron-promoted C−H activation. Although the OS mechanism for SOD activity of **1** resulted in slower rates of reaction (with the magnitude of $10^6$ $M^{-1}$ $s^{-1}$) than the IS mechanism in the case of pentaazamacrocyclic SOD mimetics (with the magnitude of $10^7$ $s^{-1}$),[67] the results here show that the heavy use of this pathway limits the formation of deleterious $OH^\bullet$ and $Mn^{IV}$-oxo species.

To summarize, we have determined important factors that regulate SOD catalysis through both inner- and outer-sphere mechanisms. The steric bulk and charge distribution of the polydentate ligand regulate the operation of inner- or outer-sphere mechanisms. Metal-bound water molecules both facilitate the PCET necessary for OS pathways and determine the feasibility of competing OS and IS mechanisms through coordination equilibria. The importance of the water ligand contrasts sharply with the traditional view of active-site water molecules merely serving as place-holders for other reagents in bioinorganic chemistry.

## ASSOCIATED CONTENT

**ⓈSupporting Information**

The Supporting Information is available free of charge on the ACS Publications website at DOI: 10.1021/jacs.6b08394.

> Crystallographic data for $[(L^{O-})Mn^{II}](ClO_4)\cdot1.5H_2O$ in CIF format (CIF)
> Crystallographic data for $[(L^{OH})Mn^{II}(OAc)](ClO_4)\cdot nH_2O$ in CIF format (CIF)
> Additional experimental procedures; detailed description of data treatment of water exchange measurements; details concerning the speciation of $[(L^{OH})Mn^{II}(solv)]-(ClO_4)_2$ (**1**) below pH 6; and additional data concerning X-ray crystallography, electrochemistry, SOD activity, oxygen reduction, quantum chemical methods (including Cartesian coordinates), ROS detection by EPR and TNB, CSI-MS, and magnetic measurements (PDF)

## AUTHOR INFORMATION

**Corresponding Authors**
*crg0005@auburn.edu
*ivana.ivanovic@chemie.uni-erlangen.de

**ORCID** 🆔
Jens Langer: 0000-0002-2895-4979
Christian R. Goldsmith: 0000-0001-7293-1267
Ivana Ivanović-Burmazović: 0000-0002-1651-3359

**Notes**
The authors declare no competing financial interest.

## REFERENCES

(1) Karlin, K. D.; Lippard, S. J.; Valentine, J. S.; Burrows, C. J. *Acc. Chem. Res.* **2015**, *48*, 2659.

(2) Groni, S.; Hureau, C.; Guillot, R.; Blondin, G.; Blain, G.; Anxolabéhère-Mallart, E. *Inorg. Chem.* **2008**, *47*, 11783.

(3) Jackson, T. A.; Gutman, C. T.; Maliekal, J.; Miller, A.-F.; Brunold, T. C. *Inorg. Chem.* **2013**, *52*, 3356.

(4) Miller, A.-F. *Acc. Chem. Res.* **2008**, *41*, 501.

(5) Grove, L. E.; Xie, J.; Yikilmaz, E.; Miller, A.-F.; Brunold, T. C. *Inorg. Chem.* **2008**, *47*, 3978.

(6) Jackson, T. A.; Brunold, T. C. *Acc. Chem. Res.* **2004**, *37*, 461.

(7) Riley, D. P. *Chem. Rev.* **1999**, *99*, 2573.

(8) Riley, D. P.; Lennon, P. J.; Neumann, W. L.; Weiss, R. H. *J. Am. Chem. Soc.* **1997**, *119*, 6522.

(9) Hureau, C.; Blanchard, S.; Nierlich, M.; Blain, G.; Rivière, E.; Girerd, J.-J.; Anxolabéhère-Mallart, E.; Blondin, G. *Inorg. Chem.* **2004**, *43*, 4415.

(10) Stallings, W. C.; Pattridge, K. A.; Strong, R. K.; Ludwig, M. L. *J. Biol. Chem.* **1984**, *259*, 10695.

(11) Yu, M.; Beyers, R. J.; Gorden, J. D.; Cross, J. N.; Goldsmith, C. R. *Inorg. Chem.* **2012**, *51*, 9153.

(12) Yu, M.; Ambrose, S. L.; Whaley, Z. L.; Fan, S.; Gorden, J. D.; Beyers, R. J.; Schwartz, D. D.; Goldsmith, C. R. *J. Am. Chem. Soc.* **2014**, *136*, 12836.

(13) Sheng, Y.; Stich, T. A.; Barnese, K.; Gralla, E. B.; Cascio, D.; Britt, R. D.; Cabelli, D. E.; Valentine, J. S. *J. Am. Chem. Soc.* **2011**, *133*, 20878.

(14) Sheng, Y.; Butler Gralla, E.; Schumacher, M.; Cascio, D.; Cabelli, D. E.; Valentine, J. S. *Proc. Natl. Acad. Sci. U. S. A.* **2012**, *109*, 14314.

(15) Sheng, Y.; Abreu, I. A.; Cabelli, D. E.; Maroney, M. J.; Miller, A.-F.; Teixeira, M.; Valentine, J. S. *Chem. Rev.* **2014**, *114*, 3854.

(16) Salvemini, D.; Wang, Z.-Q.; Zweier, J. L.; Samouilov, A.; Macarthur, H.; Misko, T. P.; Currie, M. G.; Cuzzocrea, S.; Sikorski, J. A.; Riley, D. P. *Science* **1999**, *286*, 304.

(17) Friedel, F. C.; Lieb, D.; Ivanovic-Burmazovic, I. *J. Inorg. Biochem.* **2012**, *109*, 26.

(18) Zuberbühler, A. D.; Kaden, T. A. *Talanta* **1982**, *29*, 201.

(19) Zahl, A.; Neubrand, A.; Aygen, S.; van Eldik, R. *Rev. Sci. Instrum.* **1994**, *65*, 882.

(20) *CrysAlis^{Pro}*, version 1.171.38.43; Rigaku Oxford Diffraction, Yarnton, England, 2016.

(21) Dolomanov, O. V.; Bourhis, L. J.; Gildea, R. J.; Howard, J. A. K.; Puschmann, H. *J. Appl. Crystallogr.* **2009**, *42*, 339.

(22) Sheldrick, G. M. *Acta Crystallogr., Sect. A: Found. Adv.* **2015**, *71*, 3.

(23) Sheldrick, G. M. *Acta Crystallogr., Sect. A: Found. Crystallogr.* **2008**, *64*, 112.

(24) Perdew, J. P.; Chevary, J. A.; Vosko, S. H.; Jackson, K. A.; Pederson, M. R.; Singh, D. J.; Fiolhais, C. *Phys. Rev. B: Condens. Matter Mater. Phys.* **1992**, *46*, 6671.

(25) Perdew, J. P.; Chevary, J. A.; Vosko, S. H.; Jackson, K. A.; Pederson, M. R.; Singh, D. J.; Fiolhais, C. *Phys. Rev. B: Condens. Matter Mater. Phys.* **1993**, *48*, 4978.

(26) Perdew, J. P.; Burke, K.; Wang, Y. *Phys. Rev. B: Condens. Matter Mater. Phys.* **1996**, *54*, 16533.

(27) Lee, C.; Yang, W.; Parr, R. G. *Phys. Rev. B: Condens. Matter Mater. Phys.* **1988**, *37*, 785.

(28) Stephens, P. J.; Devlin, F. J.; Chabalowski, C. F.; Frisch, M. J. *J. Phys. Chem.* **1994**, *98*, 11623.

(29) Becke, A. D. *J. Chem. Phys.* **1993**, *98*, 5648.

(30) Puchta, R.; Dahlenburg, L.; Clark, T. *Chem. - Eur. J.* **2008**, *14*, 8898.

(31) Selçuki, C.; van Eldik, R.; Clark, T. *Inorg. Chem.* **2004**, *43*, 2828.

(32) Weigend, F.; Ahlrichs, R. *Phys. Chem. Chem. Phys.* **2005**, *7*, 3297.

(33) Weigend, F. *Phys. Chem. Chem. Phys.* **2006**, *8*, 1057.

(34) Eichkorn, K.; Treutler, O.; Öhm, H.; Häser, M.; Ahlrichs, R. *Chem. Phys. Lett.* **1995**, *240*, 283.

(35) Eichkorn, K.; Weigend, F.; Treutler, O.; Ahlrichs, R. *Theor. Chem. Acc.* **1997**, *97*, 119.

(36) Frisch, M. J.; Trucks, G. W.; Schlegel, H. B.; Scuseria, G. E.; Robb, M. A.; Cheeseman, J. R.; Scalmani, G.; Barone, V.; Mennucci, B.; Petersson, G. A.; Nakatsuji, H.; Caricato, M.; Li, X.; Hratchian, H. P.; Izmaylov, A. F.; Bloino, J.; Zheng, G.; Sonnenberg, J. L.; Hada, M.; Ehara, M.; Toyota, K.; Fukuda, R.; Hasegawa, J.; Ishida, M.; Nakajima, T.; Honda, Y.; Kitao, O.; Nakai, H.; Vreven, T.; Montgomery, J. A., Jr.; Peralta, J. E.; Ogliaro, F.; Bearpark, M. J.; Heyd, J.; Brothers, E. N.; Kudin, K. N.; Staroverov, V. N.; Kobayashi, R.; Normand, J.; Raghavachari, K.; Rendell, A. P.; Burant, J. C.; Iyengar, S. S.; Tomasi, J.; Cossi, M.; Rega, N.; Millam, N. J.; Klene, M.; Knox, J. E.; Cross, J. B.; Bakken, V.; Adamo, C.; Jaramillo, J.; Gomperts, R.; Stratmann, R. E.; Yazyev, O.; Austin, A. J.; Cammi, R; Pomelli, C.; Ochterski, J. W.; Martin, R. L.; Morokuma, K.; Zakrzewski, V. G.; Voth, G. A.; Salvador, P.; Dannenberg, J. J.; Dapprich, S.; Daniels, A. D.; Farkas, Ö.; Foresman, J. B.; Ortiz, J. V.; Cioslowski, J.; Fox, D. J. *Gaussian 09*; Gaussian, Inc.: Wallingford, CT, 2009.

(37) Gale, E. M.; Mukherjee, S.; Liu, C.; Loving, G. S.; Caravan, P. *Inorg. Chem.* **2014**, *53*, 10748.

(38) Lieb, D.; Friedel, F. C.; Yawer, M.; Zahl, A.; Khusniyarov, M. M.; Heinemann, F. W.; Ivanović-Burmazović, I. *Inorg. Chem.* **2013**, *52*, 222.

(39) Dees, A.; Zahl, A.; Puchta, R.; van Eikema Hommes, N. J. R.; Heinemann, F. W.; Ivanović-Burmazović, I. *Inorg. Chem.* **2007**, *46*, 2459.

(40) Drahoš, B.; Kotek, J.; Hermann, P.; Lukeš, I.; Tóth, E. *Inorg. Chem.* **2010**, *49*, 3224.

(41) Maigut, J.; Meier, R.; Zahl, A.; van Eldik, R. *J. Am. Chem. Soc.* **2008**, *130*, 14556.

(42) Deeth, R. J. *Inorg. Chem.* **2008**, *47*, 6711.

(43) Trifunović, S. R.; Matović, Z. D.; Milovanović, V.; Kawaguchi, H.; Yamasaki, M. *Transition Met. Chem.* **2000**, *25*, 680.

(44) Wang, X. F.; Gao, J.; Wang, J.; Zhang, Z. H.; Wang, Y. F.; Chen, L. J.; Sun, W.; Zhang, X. D. *J. Struct. Chem.* **2008**, *49*, 724.

(45) Wu, X.; Seo, M. S.; Davis, K. M.; Lee, Y.-M.; Chen, J.; Cho, K.-B.; Pushkar, Y. N.; Nam, W. *J. Am. Chem. Soc.* **2011**, *133*, 20088.

(46) Parsell, T. H.; Behan, R. K.; Green, M. T.; Hendrich, M. P.; Borovik, A. S. *J. Am. Chem. Soc.* **2006**, *128*, 8728.

(47) Chen, J.; Yoon, H.; Lee, Y.-M.; Seo, M. S.; Sarangi, R.; Fukuzumi, S.; Nam, W. *Chem. Sci.* **2015**, *6*, 3624.

(48) Liu, G.-F.; Dürr, K.; Puchta, R.; Heinemann, F. W.; van Eldik, R.; Ivanović-Burmazović, I. *Dalton Trans.* **2009**, 6292.

(49) Ivanović-Burmazović, I.; Filipovic, M. R. *Adv. Inorg. Chem.* **2012**, *64*, 53.

(50) Ivanović-Burmazović, I. *Adv. Inorg. Chem.* **2008**, *60*, 59.

(51) Ivanovic-Burmazovic, I.; van Eldik, R. *Dalton Trans.* **2008**, 5259.

(52) Aston, K.; Rath, N.; Naik, A.; Slomczynska, U.; Schall, O. F.; Riley, D. P. *Inorg. Chem.* **2001**, *40*, 1779.

(53) Liu, G.-F.; Filipović, M.; Heinemann, F. W.; Ivanović-Burmazović, I. *Inorg. Chem.* **2007**, *46*, 8825.

(54) Goldsmith, C. R.; Cole, A. P.; Stack, T. D. P. *J. Am. Chem. Soc.* **2005**, *127*, 9904.

(55) Hubin, T. J.; McCormick, J. M.; Alcock, N. W.; Busch, D. H. *Inorg. Chem.* **2001**, *40*, 435.

(56) Ivanović-Burmazović, I.; Jelković, K. *Adv. Inorg. Chem.* **2004**, *55*, 315.

(57) Lassalle-Kaiser, B.; Hureau, C.; Pantazis, D. A.; Pushkar, Y.; Guillot, R.; Yachandra, V. K.; Yano, J.; Neese, F.; Anxolabéhère-Mallart, E. *Energy Environ. Sci.* **2010**, *3*, 924.

(58) Würtele, C.; Gaoutchenova, E.; Harms, K.; Holthausen, M. C.; Sundermeyer, J.; Schindler, S. *Angew. Chem., Int. Ed.* **2006**, *45*, 3867.

(59) Groni, S.; Blain, G.; Guillot, R.; Policar, C.; Anxolabéhère-Mallart, E. *Inorg. Chem.* **2007**, *46*, 1951.

(60) Lieb, D.; Zahl, A.; Shubina, T. E.; Ivanović-Burmazović, I. *J. Am. Chem. Soc.* **2010**, *132*, 7282.

(61) Riley, D. P.; Schall, O. F. *Adv. Inorg. Chem.* **2006**, *59*, 233.

(62) Ivanović-Burmazović, I.; Hamza, M. S. A.; van Eldik, R. *Inorg. Chem.* **2006**, *45*, 1575.

(63) Groni, S.; Dorlet, P.; Blain, G.; Bourcier, S.; Guillot, R.; Anxolabéhère-Mallart, E. *Inorg. Chem.* **2008**, *47*, 3166.

(64) Lah, M. S.; Dixon, M. M.; Pattridge, K. A.; Stallings, W. C.; Fee, J. A.; Ludwig, M. L. *Biochemistry* **1995**, *34*, 1646.

(65) Miriyala, S.; Spasojevic, I.; Tovmasyan, A.; Salvemini, D.; Vujaskovic, Z.; St. Clair, D.; Batinic-Haberle, I. *Biochim. Biophys. Acta, Mol. Basis Dis.* **2012**, *1822*, 794.

(66) Haber, A.; Gross, Z. *Chem. Commun.* **2015**, *51*, 5812.

(67) Weiss, R. H.; Riley, D. P. In *Uses of Inorganic Chemistry in Medicine*; Farrell, N., Ed.; Royal Society of Chemistry: Cambridge, UK, 1999; Chapter 7.